# Same-sign $W$ pair production in composite Higgs models

Christoph Englert,[1] Peter Schichtel,[2] and Michael Spannowsky[2]

[1]SUPA, School of Physics and Astronomy, University of Glasgow, Glasgow G12 8QQ, UK
[2]Institute for Particle Physics Phenomenology, Department of Physics, Durham University, Durham DH1 3LE, UK

Non-minimal composite Higgs scenarios can contain exotic Higgs states which, if getting observed at the Large Hadron Collider, will help to constrain the underlying UV structure of the strong dynamics. Doubly charged Higgs bosons are well-motivated scalar degrees of freedom in this context. Their phenomenology in typical composite scenarios can differ from well-established Higgs triplet extensions of the SM. Related search strategies are not necessarily adapted to such a scenario as a consequence. In this paper we discuss the sensitivity reach to doubly charged Higgs bosons with decays into pairs of same-sign $W$ bosons. While production cross sections are small, we show that significant constraints on $H^{\pm\pm} \to W^{\pm}W^{\pm}$ can be obtained, providing a new opportunity to constrain the potential composite structure of the TeV scale up to $m_{H^{\pm\pm}} \simeq 800$ GeV.

## I. INTRODUCTION

After the Higgs boson discovery, followed by the lack of any conclusive hints for physics beyond the Standard Model (BSM), the hierarchy problem remains one of the most pressing nuisances that our understanding of the TeV scale faces. Although TeV scale naturalness is not a technical problem, it is surprising that the success story of perturbative quantum field theory seems to be challenged by a state whose appearance is directly linked to the TeV scale itself. Many BSM scenarios have been devised over the past decades to explain the TeV scale as a natural phenomenon either through perturbative cancellations guaranteed by approximate (super)symmetry or through dimensional trans-mutation effects. The latter adapt ideas of QCD confinement to the TeV scale with phenomenologically necessary model-building adjustments.

It is fair to say that there is a much more detailed understanding of supersymmetric extensions of the SM than there is for strongly interacting theories of the TeV scale. This is mostly due to the fact that perturbative methods are bound to break down for strongly interacting theories and phenomenological applications necessarily need to revert to chiral perturbation theory ($\chi$PT) techniques [1–3]. Although $\chi$PT is an extremely successful concept (for instance, it serves to explain the pion mass splitting [4] which acts as a blueprint for composite Higgs scenarios [4–9]), it is unclear whether UV completions of a particular low energy theory do indeed exist. This constitutes a long-standing problem in the classification of composite Higgs scenarios, which has motivated investigations using both dualities [10, 11] and lattice computations [12–14].

While UV completions of the minimal composite Higgs (MCHM) scenarios have proven difficult to construct, there are non-minimal models with known UV completions [15–18]. Typically, these non-minimal extensions predict a range of scalar [19, 20], fermionic [21] as well as potentially vectorial exotics. Among these, scalar exotics such as a doubly charged Higgs boson are tell-tale stories of the compositeness nature of the TeV scale [22].

Such states are searched for by the ATLAS and CMS experiments, either in leptonic decays, motivated from generic Higgs $SU(2)_L$ triplet extensions [23, 24], or same sign $W$ boson final states. The latter will be induced if the triplet plays a role in electroweak symmetry breaking [25–34].

In some composite Higgs scenarios there are doubly charged Higgs bosons that fall into the middle of these analysis strategies: they play no role in the vacuum misalignment which triggers electroweak symmetry breaking and their coupling to leptons is either absent or suppressed. It is the purpose of this work to close this gap and provide sensitivity estimates for signatures that are motivated from these non-minimal composite Higgs scenarios in the TeV regime.

This paper is organised as follows. To make this work self-contained, we quickly review aspects of doubly charged Higgs bosons that arise in composite Higgs scenarios in Sec. II. In Secs. III and IV, we give details of our event simulation and analysis strategy before we draw conclusions in Sec. V.

## II. MODEL AND MOTIVATION

Recently, a potential UV completion of a non-minimal composite Higgs model was introduced in [17] (see also [35]). We will use this scenario as our main motivation for a search $H^{\pm\pm} \to W^{\pm}W^{\pm}$. The model of Ref. [17] is based on the symmetry group

$$\underbrace{SU(4)}_{H_c} \times \underbrace{SU(5) \times SU(3) \times SU(3)' \times U(1)_X \times U(1)'}_{G_F}, \tag{1}$$

with fermions transforming as $\psi \in \mathbf{6}, \chi \in \mathbf{4}, \tilde{\chi} \in \bar{\mathbf{4}}$ under the "hyper colour" gauge group $H_c = SU(4)$. Strong $SU(4)$ dynamics cause the breakdown of the global symmetries $G_F$

$$SU(5) \to SO(5) , \tag{2}$$

and

$$SU(3) \times SU(3)' \to SU(3), \tag{3}$$

as well as the breaking of $U(1)'$. The author of [17] argues that Eq. (2) occurs at a higher scale than Eq. (3); the low energy effective theory can then be parametrised by the coset

$$G_F/H_F = \frac{SU(5)}{SO(5)} \times \frac{SU(3) \times SU(3)'}{SU(3)} \times U(1)' . \tag{4}$$

The unbroken global symmetry group $H_F$ contains the subgroup

$$H_F \supset SU(3)_c \times SU(2)_L \times SU(2)_R \times U(1)_X , \tag{5}$$

which can be weakly gauged to arrive at the SM gauge structure.

The symmetry breaking pattern leaves a number of distinct exotics in the theory's spectrum (for instance there is a "hypergluon" [36–38] and an inert singlet). Our analysis targets the enlarged Higgs spectrum compared to MCHM4 [7] or MCHM5 [39]. The Nambu Goldstone bosons that arise from $SU(5) \to SO(5)$ transform under $SU(2)_L \times U(1)_Y$ as

$$\mathbf{1}_0 + \mathbf{2}_{\pm 1/2} + \mathbf{3}_0 + \mathbf{3}_{\pm 1} , \tag{6}$$

and we can interpret the $\mathbf{2}_{\pm 1/2}$ multiplet as the SM Higgs field. Weakly gauging the electroweak group as part of Eq. (5), together with the presence of a heavy top quark, induces a Coleman-Weinberg potential [40] for this multiplet, which triggers electroweak symmetry breaking as the vacuum becomes dynamically misaligned with respect to the $SU(2)_L \times U(1)_Y$ ($Y = T_R^3 + X$) preserving direction [4].

A phenomenological smoking gun of this scenario is the appearance of a $\mathbf{3}_{\pm 1}$ multiplet, which contains a doubly charged Higgs boson that, however, has no relation to the electroweak scale as vacuum misalignment proceeds entirely through $\mathbf{2}_{\pm 1/2}$ interactions. This phenomenological situation is vastly different from other Higgs triplet scenarios [24–27, 41]: firstly, tension with the $\rho$ parameter (either in custodial [42] or non-custodial realisations [41]) is relaxed and related fine-tuning is absent. Secondly, since $\mathbf{3}_{0,\pm 1}$ do not participate in electroweak symmetry breaking, they will not leave an observable signature in weak boson fusion final states [28–30, 43–45], which are particularly suited to custodial Higgs triplet models. Instead their production will need to happen through pair production [41] entirely fixed by the quantum numbers of the weak isotriplet.

With the only distinction of Eq. (4), the model of [17] follows the paradigm of the MCHM scenario; massive bottom and top quarks are included through partial compositeness [6, 46] by introducing three top partners $\{T_i\}$ and one bottom partner $B$ that lift the fundamental $t, b$ masses. Similar to MCHM5, this introduces a range of effective Higgs-fermion interactions. The interaction most relevant to the present work is given by [17]

$$\mathcal{L} \supset -\sqrt{2} i \lambda_q \, \bar{b}_L X_R H^{--} + \text{h.c.} \tag{7}$$

where $X$ denotes a top partner with charge 5/3 that is characteristic for custodial symmetry preserving composite Higgs scenarios [21].* The $X$ field together with four other top-like fields in



FIG. 1: Typical Feynman diagram contributing to the decay $H^{--} \to W^- W^-$ in the Lagrangian eigenbasis.

MCHM5 forms a charged current that couples to the $W$ field. The decay of the doubly charged Higgs boson into same sign $W$s, albeit absent at tree-level, hence proceeds at loop level through including a mass insertion, as indicated in Fig. 1. This decay is therefore directly related to the mixing angles that generate the physical $b$ quark mass†.
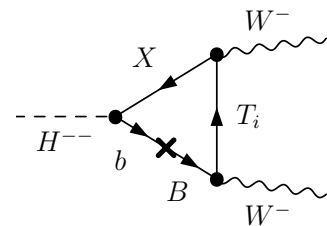
———

\* Note that the chirality structure of the interaction Eq. (7) will induce higher-dimensional CP-violating effective interactions, see below. Similar loop-induced effects are present in the SM as well.

† This is similar to the decay $H \to \gamma\gamma, gg$ in the SM, with the photons and gluons standing in no relation to spontaneous symmetry breaking.

Note, that there is also the possibility of this decay to be anomaly term induced [35] with a different CP and Lorentz structure.[‡] In practice the decay amplitude can be evaluated through rotating the top quark partners to the mass-eigenbasis which results in a non-diagonal coupling structure of the $W$ in the space of top and bottom quarks. The very decay of the doubly charged Higgs into same sign $W$ therefore carries a lot of (although degenerate) information about the particular structure of mass generation through partial compositeness.

Numerically there is only a small mixing required to lift an elementary fermion to the mass of the bottom quark, and in general one expects that the decay amplitude is parametrically small (in line with the effective field theory analysis of [47]). The difference compared to the minimal composite scenarios in the present case, however, is the potential absence of low-energy two-body final states that allow a prompt and charge-conserving $H^{\pm\pm}$ decay.[§]

While details of the doubly charged Higgs decays are certainly model-dependent and maybe even beyond perturbative control (we will come back to interpreting our results below in terms of composite scenarios later), it is clear that any statistical significant observation or exclusion of $H^{\pm\pm} \to W^\pm W^\pm$ leading to a distinctive resonant final state

$$l^+ l^+ l^- l^- \not{E}_T \,, \tag{8}$$

with Higgs masses in the multi-hundred GeV regime, will have strong implications for the underlying effective description of the compositeness model, with direct ramifications for its underlying UV structure (e.g. through the mixing effects in Fig. 1).

This particular final state is not plagued by large QCD backgrounds, but signal cross sections are generically small [49, 50]. Including estimates for charge mis-tagging etc. is therefore important to arrive a at realistic expectation of the sensitivity to this model. Taking the pNGB character of the Higgs boson at face value, we can expect that the doubly charged Higgs boson is heavy and we will leave its mass as a free parameter $m_{H^{\pm\pm}} > 125$ GeV in our analysis. In particular, we will compare the performance of various analysis approaches that make use of large discriminative power for the expected small signal vs. background ratio for large doubly charged Higgs masses.

## III. EVENT SIMULATION

Focusing on the leptonic $W$ decay modes we consider Eq. (8) as final state signature, where the $\not{E}_T$ stems from four neutrinos in the final state and $l \in \{e, \mu\}$. As Eq. (8) describes a very clean channel at the LHC, the only irreducible backgrounds we consider are $W^+W^+W^-W^-$, four lepton production in association with a $Z$, and two leptons together with $W^+W^-$. All other backgrounds are reducible. We identify jet fakes, i.e a jet being mistaken as a lepton, as the main source of such events. The fake rate we control via [51]

$$\mathrm{P}\,(j \to e) = 0.0048 \times \exp\left[-0.035 \times \frac{p_{T,j}}{\mathrm{GeV}}\right] \,, \tag{9}$$

for all jets within the reach of the electromagnetic calorimeter. In practice, we explore jets clustered with the anti-$k_T$ algorithm, as implemented in FastJet [52], with a radius parameter of $R = 0.4$ and $p_T^{\min} \geq 10$ GeV. Therefore, the highest probability to fake an electron is given by low momentum jets $\mathrm{P}^{\max}\,(j \to e) = 3.4 \times 10^{-3}$. This gives us a direct handle to estimate whether a certain reducible background with a given cross section is important for our study. Two leptons plus $W^\pm$ and jet production provide candidate events for such a background, as well as Drell Yan in association with at least two jets, for which the jets need to fake the number of missing leptons. Similarly, lepton neutrino production with three jets need to be included as well. In principle, QCD-induced jet production contributes too, however, requiring at least one muon in the final state, we render the latter one irrelevant, while keeping 93% of the signal.

Top quark production constitutes a further category of backgrounds. We consider $t\bar{t}$ production in association with either $W^+W^-$ or $l^+l^-$. When there are $B$ mesons in the final state we need to take the $b$ mis-tagging rate into account as well. We assume the tagging rate to be 70% per true $b$-jet [53, 54]; a $b$ veto results in an efficiency factor of 0.09.

Due to inherent and fake missing energy in QCD jet radiation we study the production of four leptons as last class of backgrounds in our list of dominant backgrounds. As we do not include a full detector simulation, we need to

---

[‡] We are grateful to Gabriele Ferretti for pointing out this possibility.

[§] The composite dynamics that will create a dynamical mass for $H^{--}$ will also lift $H^-$ and mass splittings can occur inside the $T_L^3 = 1$ multiplet or between the $|Y| = 0, 1$ multiplets. However, unless the strong dynamics changes the picture radically (which need to be assessed on the lattice), the mass splittings should be entirely perturbative and qualitatively similar to the $\pi^\pm - \pi^0$ mass splitting. From the perspective of chiral perturbation theory cascade decays $H^{++} \to H^+ H^+$ seem unlikely. Current constraints exclude top partners in the range of 600 GeV [48]. We therefore assume $m_X > m_{H^{\pm\pm}}$ in the following.

model the amount of missing energy. It has been shown that

$$\frac{\Delta \not{E}_T}{\not{E}_T} = \frac{2.92}{\not{E}_T} - 0.07 \tag{10}$$

corresponds to a conservative estimate [55]. Therefore, we smear the missing energy vector as computed from Monte-Carlo truth with a gaussian distribution according to Eq. (10) instead of modeling the detector response to every single final state particle.

A further obstacle in describing the final state is charge miss identification. As for the electron fakes we use a transverse momentum dependent description [56]

$$P\,(\text{charge flip}) = \min\left(0.2,\ 4.68 \times 10^{-8} \left[\frac{p_T}{\text{GeV}} + 65.0\right]^2\right), \tag{11}$$

and we ignore the possibility of a charge flip for muons. Equation (11) results from fitting a parabola to the data points that we have extrapolated from Ref. [56]. We checked that the results presented in this paper do not show a significant dependence on the exact result of this fit.

As we are interested in the main kinematic features of the relevant channels, we simulate all processes at their respective leading order (LO). We use `MadGraph_aMCatNLO` [57, 58] to generate matrix element level results for our model and `Herwig 7`'s [59] angular ordered parton shower [60] for showering and decays. For the simulation of the background we employ `MadGraph_aMCatNLO`'s LO amplitudes interfaced to the `Herwig 7` generator, again using the angular ordered parton shower, with `Herwig 7` taking care of all decays [61–63]. Since QCD details are not too important for this particular clean final state apart from changed normalisations (see below), we do not include hadronization and underlying event (UE) effects. Indeed, we checked that including UE has no influence on the lepton separation for our signal process.

In Tab. I we collect the simulated processes as well as their cross section on generator level $\sigma_{\text{MC}}$. The fiducial cross sections for $l^+l^+l^-l^-Z$, $t\bar{t}W^+W^-$, and $l^\pm \nu jjj$ are indeed so small that we do not need to consider them any further.

For some of the processes next-to-leading order (NLO) corrections are large. In our MC generation we therefore include the following flat $K = \sigma^{\text{NLO}}/\sigma^{\text{LO}}$-factors: 1.3 for all signal processes due to a Drell-Yan character (e.g. [64, 65]), 2.0 for $W^+W^+W^-W^-$ (conservatively adopted from $WWZ$ production [66–68]) and $l^+l^-W^+W^-$ [66–68] as well as 1.6 for $l^+l^+l^-l^-$ [69, 70] and $l^+l^-W^\pm j$ [71, 72]. For all other processes we neglect any NLO corrections as they turn out to be negligible contributions to the background.

## IV. ANALYSIS

To analyse and identify kinematic regimes from which our doubly charged heavy Higgs (we will just use Higgs as abbreviation from now on) signal might be extracted, we first need to define a fiducial region using a set of acceptance cuts. We ask for at least four leptons in the final state; two of them have positive charge (+) while the other two have to have negative charge (−). This results in a cut efficiency $\epsilon_{++--}$. For the four leptons we require acceptance cuts staggered in $p_T$ as follows

$$p_{T,l}^{\text{leading}} \geq 20 \text{ GeV} \qquad p_{T,l}^{\text{second}} \geq 18 \text{ GeV} \qquad p_{T,l}^{\text{third}} \geq 15 \text{ GeV} \qquad p_{T,l}^{\text{fourth}} \geq 10 \text{ GeV} \tag{12}$$

as well as $|\eta_l| \leq 2.5$. Thies yields a further efficiency $\epsilon_{\text{acceptance}}$. As many of the background processes contain resonant $Z$ production we require opposite sign, same flavor leptons to have an invariant mass above 96 GeV.

$$m_{e^+e^-|\mu^+\mu^-} \geq 96.0 \text{ GeV}, \tag{13}$$

which also efficiently removes the photon contribution in these events and yields a further efficiency factor $\epsilon_{Z\text{-peak}}$. Furthermore, as QCD contributes to our missing energy we use the anti-$k_T$ algorithm, as implemented in `FastJet`, with radius parameter $R = 0.4$, a minimum transverse momentum $p_T^{\text{min}} = 20$ GeV, and $|\eta_j| \leq 4.5$ to obtain well defined jets. The missing energy vector is then computed from

$$\vec{\not{p}}_T = \sum_{i \in l,j} \vec{p}_{T,i} \tag{14}$$

and, in addition, exposed to Eq. (10). In Tab. I we collect the cut efficiencies $\epsilon$ and the fiducial cross section $\sigma_{\text{fiducial}}$ after applying Eq. (12), Eq. (13) and requiring at least one muon.

| process | $W^+W^+W^-W^-$ | $l^+l^+l^-l^-Z$ | $l^+l^+l^-l^-$ | $l^+l^-W^+W^-$ | $t\bar{t}W^+W^-$ | $t\bar{t}l^+l^-$ |
|---|---|---|---|---|---|---|
| $\sigma_{\text{MC}}$[ab] | 2.2 | 13 | 21 | 538 | 11 | $1.2 \times 10^3$ |
| $\epsilon_{\text{four leptons}}$ | 0.62 | 0.71 | 0.37 | 0.52 | $0.32 \times 10^{-2}$ | $0.30 \times 10^{-2}$ |
| $\epsilon_{++--}$ | 0.62 | 0.70 | 0.37 | 0.52 | $0.31 \times 10^{-2}$ | $0.29 \times 10^{-2}$ |
| $\epsilon_{\text{acceptance}}$ | 0.56 | 0.69 | 0.36 | 0.48 | $0.27 \times 10^{-2}$ | $0.26 \times 10^{-2}$ |
| $\epsilon_{Z\text{-peak}}$ | 0.26 | 0.0062 | 0.0050 | 0.035 | $0.11 \times 10^{-2}$ | $0.14 \times 10^{-3}$ |
| $\sigma_{\text{fiducial}}$[ab] | 0.58 | 0.081 | 0.10 | 19 | 0.013 | 0.17 |

| process | $l^+l^-\nu\nu jj$ | $l^\pm\nu jjj$ | $l^+l^-W^\pm j$ | $l^+l^-jj$ |
|---|---|---|---|---|
| $\sigma_{\text{MC}}$[ab] | $15 \times 10^6$ | $2.6 \times 10^9$ | $0.59 \times 10^6$ | $69 \times 10^6$ |
| $\epsilon_{\text{four leptons}}$ | $0.81 \times 10^{-5}$ | $0.45 \times 10^{-8}$ | $0.13 \times 10^{-2}$ | $0.18 \times 10^{-5}$ |
| $\epsilon_{++--}$ | $0.45 \times 10^{-5}$ | $0.18 \times 10^{-8}$ | $0.68 \times 10^{-3}$ | $0.93 \times 10^{-6}$ |
| $\epsilon_{\text{acceptance}}$ | $0.37 \times 10^{-5}$ | $0.87 \times 10^{-9}$ | $0.62 \times 10^{-3}$ | $0.69 \times 10^{-6}$ |
| $\epsilon_{Z\text{-peak}}$ | $0.19 \times 10^{-6}$ | $0.17 \times 10^{-10}$ | $0.21 \times 10^{-3}$ | $0.40 \times 10^{-7}$ |
| $\sigma_{\text{fiducial}}$[ab] | 2.7 | 0.039 | 130 | 2.6 |

| $m_H$[GeV] | 200 | 300 | 400 | 500 | 600 | 700 | 800 | 900 | 1000 |
|---|---|---|---|---|---|---|---|---|---|
| $\sigma_{\text{MC}}$[ab] | 205 | 87 | 42 | 22 | 12.4 | 7.3 | 4.6 | 2.9 | 1.8 |
| $\epsilon_{\text{four leptons}}$ | 0.71 | 0.77 | 0.80 | 0.83 | 0.84 | 0.85 | 0.86 | 0.86 | 0.87 |
| $\epsilon_{++--}$ | 0.71 | 0.76 | 0.80 | 0.82 | 0.83 | 0.84 | 0.85 | 0.85 | 0.85 |
| $\epsilon_{\text{acceptance}}$ | 0.63 | 0.68 | 0.71 | 0.74 | 0.76 | 0.77 | 0.77 | 0.78 | 0.79 |
| $\epsilon_{Z\text{-peak}}$ | 0.32 | 0.40 | 0.48 | 0.54 | 0.58 | 0.61 | 0.64 | 0.66 | 0.68 |
| $\sigma_{\text{fiducial}}$[ab] | 66 | 36 | 20 | 12 | 7.2 | 4.5 | 2.9 | 1.9 | 1.2 |

TABLE I: List of background and signal processes considered in this study. First row: $\sigma_{\text{MC}}$ is the cross section at generator level. Additional rows: cut efficiencies (subsequent efficiencies are included multiplicatively, for more details see text). Last row: $\sigma_{\text{fiducial}}$ is the cross section after all acceptance cuts as used for the analysis section.

## A. Naive Cut and Count

When analysing the significance of a possible signal or excluding its existence with a given level of certainty different test statistics may be used. In our case we implement a simple counting approach based on a Poisson distribution. Given a sample of expected signal (S) and background (B) events, the significance $Z$ is given by

$$Z = \frac{\text{S}}{\sqrt{\text{S} + \text{B}}} \, . \tag{15}$$

Sometimes $\text{S}/\sqrt{\text{B}}$ is used as well. However, we emphasize that for low background cross sections, as we face in our study, this leads to wrong conclusions. Take, for example, S = 1 and B = 0.1. This would yield a significance of 3, which is clearly an overestimate when only one event in total is expected. The consequence of Eq. (15) is that one needs to expect at least four signal events in the analysis region to set an exclusion limit of 95%, which can be inferred from setting $B = 0$ and $Z = 2$. As we see, this cannot be possible for the very high mass regime of our model, even when considering the 3 ab$^{-1}$ high luminosity LHC option. However, for completeness we will show results up to $m_{H^{\pm\pm}} = 1000$ GeV.

It is also possible to invert Eq. (15), leading to

$$\mathcal{L} = \frac{Z^2 (\sigma_{\text{S}} + \sigma_{\text{B}})}{\sigma_{\text{S}}^2} \, . \tag{16}$$
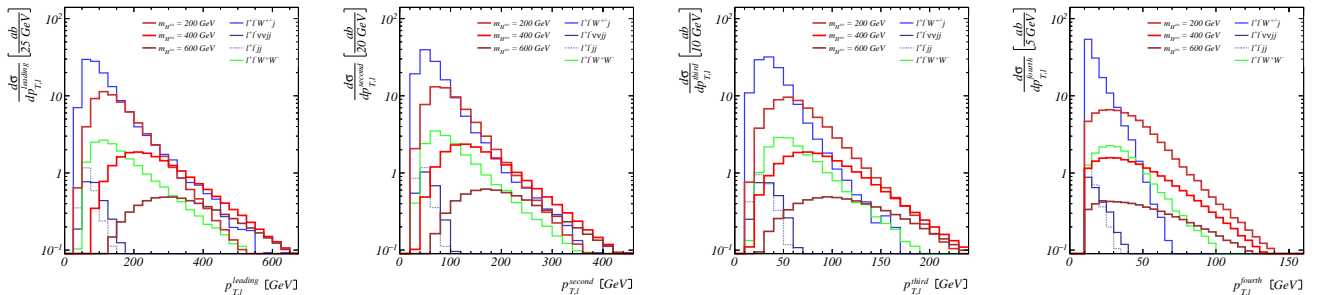
FIG. 2: Transverse momentum of the leptons sorted by $p_T$ after Eq. (12). Red: signal with $m_{H^{\pm\pm}} \in [200, 400, 600]$ GeV. Blue: Backgrounds from jets faking electrons. Green: irreducible backgrounds.

For given signal and background cross sections setting $Z \equiv 2$ yields the expected luminosity needed for an exclusion at 95% confidence level.

For this first part of our analysis we assume the branching ratio Higgs to $WW$ to be unity. Under this assumption we check observables which should yield discriminative power one by one. As the dominant backgrounds are driven by QCD radiation mistaken for electrons or an electroweak topology with masses well below 100 GeV while our signal stems from a heavy decay, the $p_T$ spectra should provide a sensitive discriminant. In Fig. 2 we show the $p_T$ for all backgrounds and a sub-sample of the Higgs mass parameter space. Note that backgrounds not listed in the legend of the plot are too small to be considered. We find that the QCD-induced backgrounds fall more steeply than the signal, see e.g. $p_{T,l}^{\text{third}}$ of $l^+l^-jj$ or $p_{T,l}^{\text{fourth}}$ of $l^+l^-W^\pm j$.

We note that despite the fact that the $1/p_T$ divergence of QCD shows itself in $p_{T,l}^{\text{third}}$ and $p_{T,l}^{\text{fourth}}$, these do not yield much discriminating power. Therefore, for the further analysis steps, we fix $p_{T,l}^{\text{third}} = 20$ GeV, $p_{T,l}^{\text{fourth}} = 15$ GeV and manipulate the leading leptons' transverse momenta to obtain a signal efficiency of $\epsilon_S = 0.9$. We tabulate the $p_T$ cuts needed for this together with the resulting background cross section $\sigma_B$ in Tab. II.

The leptonic decay of the $W$'s in the signal channel results in missing energy. Furthermore, we expect the jet radiation pattern to be sensitive to the presence of the electroweak decay [73, 74]. However, we find that the jet spectrum after $p_T$ cuts is not sensitive to the decay pattern. At least for the reducible backgrounds, the jet number spectrum does not resemble the correct starting point to count the number of jets following the strategy of [75]. It is known that the jet spectrum poses a good discriminator before restrictive $p_T$ cuts sculpt the distribution's shape [76], hence, it is plausible that it loses its sensitivity in the present case through decays. Also, only one out of two leading backgrounds stems from QCD; the $l^+l^-W^+W^-$ channel is expected to have a similar radiation pattern as our signal. We therefore do not use the number of jets to construct analysis cuts; this means we also do not impose a jet veto. However, if a jet veto should become necessary due to experimental reasons beyond the scope of this study, our analysis shows that this should not decrease the signal efficiency too much.

The missing energy is not very sensitive to the signal process after applying the cuts outlined in Tab. II, as can be seen from Fig. 3. The $p_T$ cuts force the QCD radiation into a regime where also jets produce a fair amount of missing energy. Thus we propose only a mild cut of

$$\not{E}_T > 20.0 \text{ GeV} . \tag{17}$$

There is another feature we can use to enhance our signal to background ratio: Many of the backgrounds contain either resonant $Z$ boson contributions or have no resonance connecting two of the leptons. Thus, we construct all possible invariant masses built out of two lepton four momenta added to each other. This yields a total of six

| $m_H$ [GeV] | 200 | 300 | 400 | 500 | 600 | 700 | 800 | 900 | 1000 |
|---|---|---|---|---|---|---|---|---|---|
| cut on $p_{T,l}^{\text{leading}}$ [GeV] | 70 | 95 | 120 | 140 | 160 | 180 | 200 | 220 | 240 |
| cut on $p_{T,l}^{\text{second}}$ [GeV] | 35 | 40 | 40 | 40 | 40 | 40 | 60 | 60 | 70 |
| $\sigma_B$ [ab] | 74 | 54 | 40 | 31 | 24 | 20 | 15 | 13 | 9.9 |

TABLE II: Transverse momentum cut on the two leading leptons to obtain an $\epsilon_S = 0.9$ working point and corresponding background cross section $\sigma_B$ for different mass parameters $m_{H^{\pm\pm}}$.
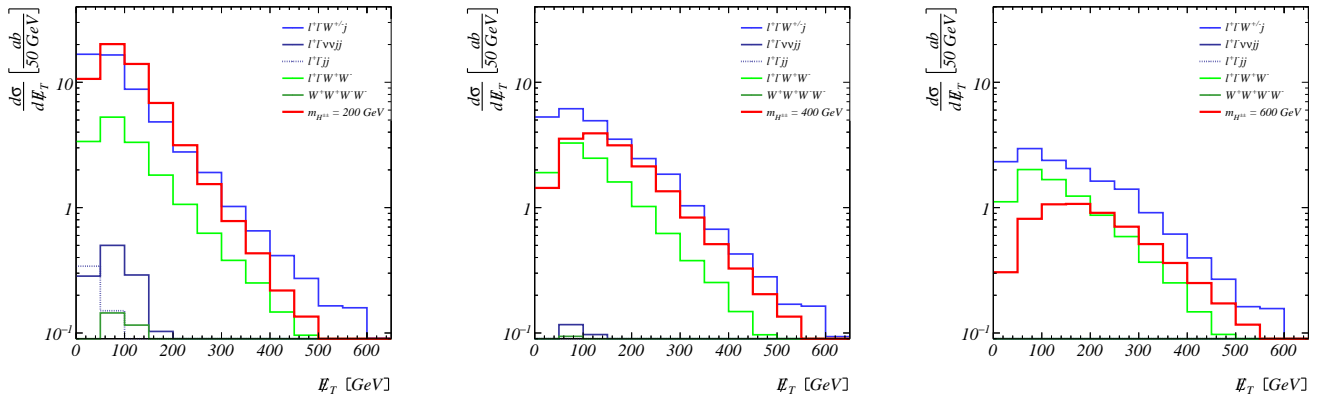
FIG. 3: Missing energy spectrum after cuts outlined in Tab. II. Red: from left to right $m_{H^{\pm\pm}} \in [200, 400, 600]$ GeV. Blue: backgrounds from jets faking electrons. Green: irreducible backgrounds.
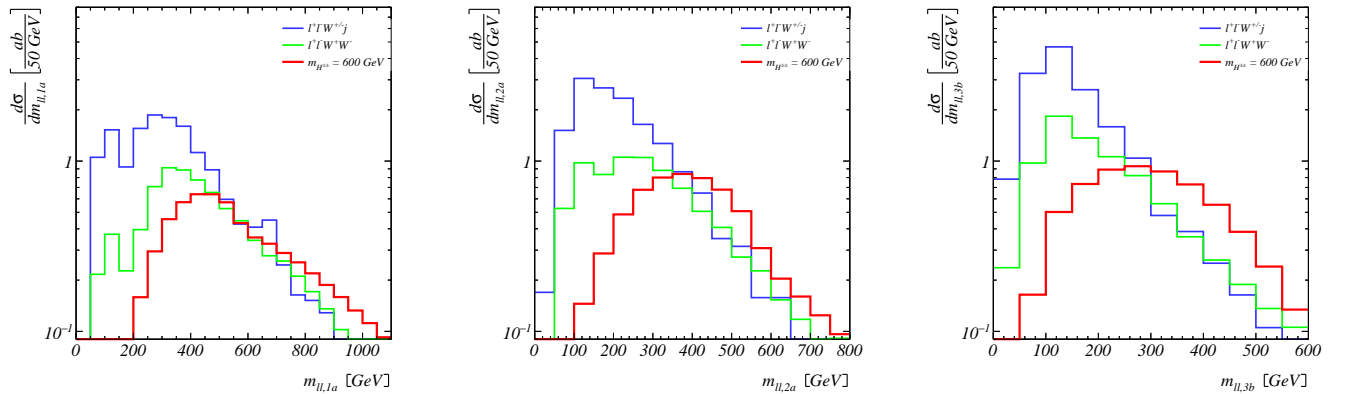


FIG. 4: Lepton pair invariant mass reconstruction after cuts outlined in Tab. II and Eq. (14). Red: signal with $m_{H^{\pm\pm}} = 600$ GeV. Blue: backgrounds from jets faking electrons. Green: irreducible backgrounds. From left to right: $m_{ll,1a}$, $m_{ll,2a}$, and $m_{ll,3b}$ (for details see text and Eq. (18))

observables.

$$m_{ll,1a} = \text{mass}\left(p_l^{\text{leading}} + p_l^{\text{second}}\right) \quad \text{and} \quad m_{ll,1b} = \text{mass}\left(p_l^{\text{third}} + p_l^{\text{fourth}}\right),$$

$$m_{ll,2a} = \text{mass}\left(p_l^{\text{leading}} + p_l^{\text{third}}\right) \quad \text{and} \quad m_{ll,2b} = \text{mass}\left(p_l^{\text{second}} + p_l^{\text{fourth}}\right),$$

$$m_{ll,3a} = \text{mass}\left(p_l^{\text{leading}} + p_l^{\text{fourth}}\right) \quad \text{and} \quad m_{ll,3b} = \text{mass}\left(p_l^{\text{second}} + p_l^{\text{third}}\right). \tag{18}$$

Interestingly, only the combinations $1a, 2a$ and $3b$ yield any additional discriminating features. We show examples for some of these for $m_{H^{\pm\pm}} = 600$ GeV in Fig. 4.

When designing the cut flow for this particular signal search, we have to balance two effects. On the one hand, we have to ensure a strong background rejection while, on the other hand, we need to ensure that the already low signal yield does not become further suppressed. For the low mass points, we find that signal and background have very similar kinematic features. We therefore suggest to not cut on the invariant lepton masses when studying the parameter space below $m_{H^{\pm\pm}} = 300$ GeV. For the rest of the parameter space we again aim for $\epsilon_S = 0.9$. We show our cut flow in Tab. III.

Since the Higgs pairs are produced back-to-back, we expect the decay products of the Higgs bosons will dominantly fall into the same detector hemispheres

$$R_{l^{\pm}l^{\pm}} = \sqrt{\Delta\eta_{l^{\pm}l^{\pm}}^2 + \Delta\phi_{l^{\pm}l^{\pm}}^2}, \tag{19}$$
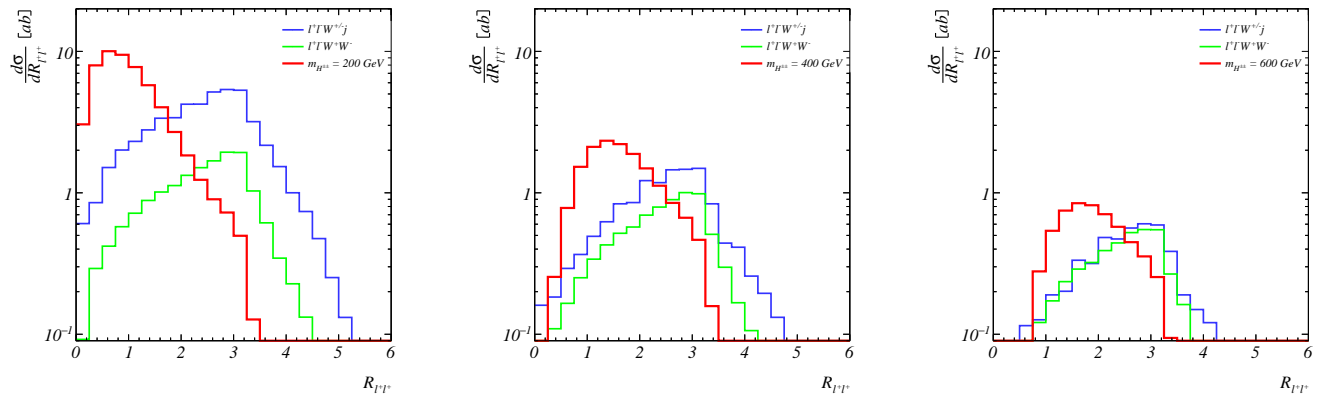
FIG. 5: Radial separation of the same sign lepton pair as defined in Eq. (19) (positive choice). Red: from left to right $m_{H^{\pm\pm}} \in [200, 400, 600]$ GeV. Blue: backgrounds from jets faking electrons. Green: irreducible backgrounds.

where $\Delta\eta$ denotes the difference in rapidity between the two leptons while $\Delta\phi$ is their azimuthal separation. In Fig 5 we show the radial distance between the same charge leptons. Indeed, these requirements are a powerful discriminator and we suggest cuts on the maximum value in Tab. III.

As we produce both Higgs bosons on-shell, the invariant mass should naively be a very good discriminator. However, since there is a fair amount of missing energy in this particular final state, we focus instead on selections of adapted definitions of the transverse mass $m_T$. There are different definitions of $m_T$ depending on the phenomenological circumstances. For instance, Ref. [77] defines

$$m_{l^{\pm}l^{\pm},T_1}^2 = \left[\sqrt{p_{l^{\pm}l^{\pm},T}^2 + m_{l^{\pm}l^{\pm}}^2} + \slashed{p}_T\right]^2 - \left[p_{l^{\pm}l^{\pm},x} + \slashed{p}_x\right]^2 - \left[p_{l^{\pm}l^{\pm},y} + \slashed{p}_y\right]^2. \tag{20}$$

and Ref. [78]

$$m_{l^{\pm}l^{\pm},T_2}^2 = \left[p_{l^{\pm}l^{\pm},T} + \slashed{p}_T\right]^2 - \left[p_{l^{\pm}l^{\pm},x} + \slashed{p}_x\right]^2 - \left[p_{l^{\pm}l^{\pm},y} + \slashed{p}_y\right]^2, \tag{21}$$

where $x$ and $y$ are simply the two coordinate axis of the transverse detector plane. The only difference between these definitions is the inclusion of the invariant lepton mass. For the case of a heavy resonance, as studied here, the former one yields better discrimination[¶]. Therefore, we show Eq. (20) for a sample of Higgs mass points in Fig. 6.

Using this $m_T$ as final discriminant, we scan along the $m_T$ axis to minimise the amount of luminosity needed for a 95% exclusion as computed from Eq. (16). We collect our results in Tab. IV. In addition we quote the discovery significance $Z$ for a $3\,\text{ab}^{-1}$ LHC, when assuming branching ratios of unity.

| $m_H$ [GeV] | 200 | 300 | 400 | 500 | 600 | 700 | 800 | 900 | 1000 |
|---|---|---|---|---|---|---|---|---|---|
| $\slashed{E}_T$ [GeV] | 20 | 20 | 20 | 20 | 20 | 20 | 20 | 20 | 20 |
| $m_{Z,1a}$ [GeV] | | 65 | 130 | 125 | 125 | 170 | 215 | 165 | 225 |
| $m_{Z,2a}$ [GeV] | | 110 | 135 | 125 | 160 | 145 | 210 | 185 | 240 |
| $m_{Z,3b}$ [GeV] | | 25 | 65 | 110 | 120 | 140 | 130 | 165 | 155 |
| $R_{l^+l^+}^{\max}$ | 2.2 | 2.3 | 2.8 | 2.8 | 2.8 | 2.8 | 2.8 | 2.8 | 2.8 |
| $\sigma_S$ [ab] | 51 | 25 | 15 | 8.8 | 5.2 | 3.2 | 2.0 | 1.3 | 0.8 |
| $\sigma_B$ [ab] | 24 | 16 | 14 | 8.8 | 6.1 | 4.4 | 3.4 | 2.6 | 2.0 |

TABLE III: Cut flow optimised for different Higgs mass scenarios. Last rows: Signal cross section $\sigma_S$ and background cross section $\sigma_B$ for different mass parameters $m_{H^{\pm\pm}}$ after the cuts stated here, see Eq. (14), Eq. (18), and Eq. (19).

---

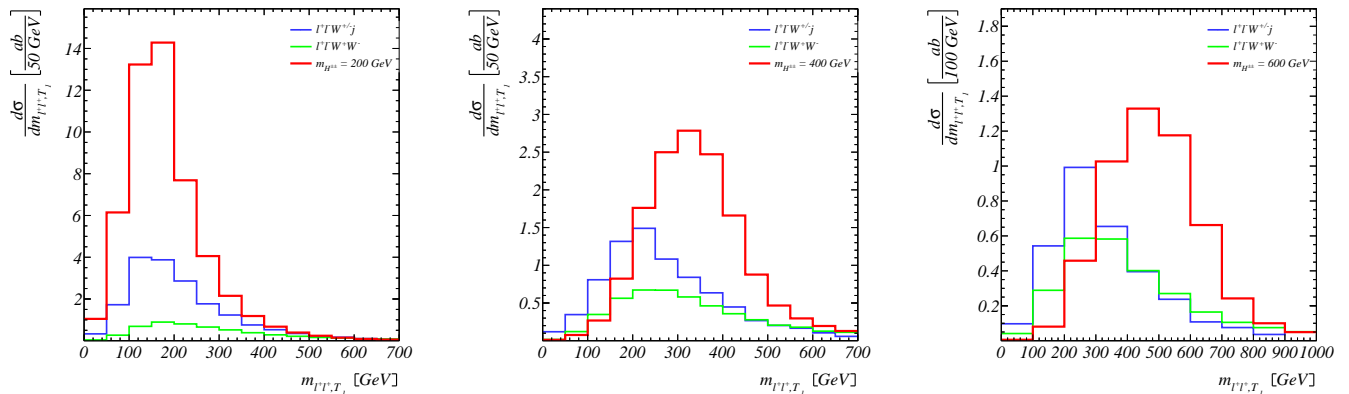[¶] Eq. (21) pushes both signal and background into the low mass region.

FIG. 6: Transverse mass after cuts outlined in Tab. III. Red: from left to right $m_{H^{\pm\pm}} \in [200, 400, 600]$ GeV. Blue: backgrounds from jets faking electrons. Green: irreducible backgrounds.

## B.   Branching Ratio $H^{\pm\pm} \to W^\pm W^\pm$ and Signal Modifier $\mu$

We can re-interpret an exclusion of unity branching ratio as a 95% confidence level constraint on the branching ratio $H^{\pm\pm} \to W^\pm W^\pm$ using the cross section for signal and background after the cuts detailed in the previous section. Eq. (16) can then be used to arrive at

$$\mathrm{BR}^4_{H^{\pm\pm} \to W^\pm W^\pm} = \frac{4\,(\sigma_\mathrm{S} + \sigma_\mathrm{B})}{\mathcal{L}\sigma_\mathrm{S}^2} \tag{22}$$

as the bound that the LHC is sensitive to at a given luminosity $\mathcal{L}$. Assuming $3\,\mathrm{ab}^{-1}$ we present our results in Tab. IV. We find that, especially for the low mass regime, branching ratios significantly smaller than unity can be probed. For the high mass regime, where the LHC has only little sensitivity, we find branching ratios greater then unity, signalising that no constraint on the underlying UV structure as motivated in Sec. II can be obtained. There a more intuitive expression as, for example, the so called signal modifier $\mu$, defined as $\sigma_\mathrm{S} \to \mu\sigma_S$, can be studied. Again starting from Eq. (16) we conclude that

$$\mu = \frac{Z^2}{2\,\mathcal{L}\,\sigma_\mathrm{S}} + \sqrt{\frac{Z^4}{4\,\mathcal{L}^2\,\sigma_\mathrm{S}^2} + \frac{Z^2\,\sigma_\mathrm{B}}{\mathcal{L}\,\sigma_\mathrm{S}^2}}\,. \tag{23}$$

Using $Z \equiv 2$ and $\mathcal{L} = 3\,\mathrm{ab}^{-1}$ we compute the upper bound for the signal modifier instead of the branching ratio. Our results can be found in Tab. IV, too.

| $m_H$ [GeV] | 200 | 300 | 400 | 500 | 600 | 700 | 800 | 900 | 1000 |
|---|---|---|---|---|---|---|---|---|---|
| cut on $m_T$ [GeV] | 2.0 | 2.0 | 173 | 234 | 280 | 341 | 367 | 457 | 488 |
| $\sigma_\mathrm{S}$ [ab] | 51 | 25 | 14 | 8.1 | 4.8 | 2.9 | 1.9 | 1.1 | 0.71 |
| $\sigma_\mathrm{B}$ [ab] | 24 | 16 | 11 | 6.1 | 3.8 | 2.3 | 1.8 | 1.1 | 0.79 |
| $\mathcal{L}$ [ab$^{-1}$] for 95% exclusion | 0.11 | 0.26 | 0.51 | 0.85 | 1.5 | 2.5 | 4.2 | 6.9 | 12 |
| $Z$ for a $3\,\mathrm{ab}^{-1}$ LHC | 10 | 6.7 | 4.8 | 3.7 | 2.8 | 2.2 | 1.7 | 1.3 | 1.0 |
| BR($H^{\pm\pm} \to W^\pm W^\pm$) | 0.44 | 0.55 | 0.64 | 0.73 | 0.84 | 0.96 | 1.1 | 1.2 | 1.4 |
| signal modifier $\mu$ | 0.12 | 0.21 | 0.33 | 0.44 | 0.63 | 0.89 | 1.3 | 1.8 | 2.7 |

TABLE IV: Signal cross section $\sigma_\mathrm{S}$ and background cross section $\sigma_\mathrm{B}$ after cut on $m_T$ (for more details see text) for different Higgs mass parameters $m_{H^{\pm\pm}}$. Last rows: target luminosity for an 95% exclusion limit, discovery significance $Z$ and upper bound on the branching ratio BR($H^{\pm\pm} \to W^\pm W^\pm$) as well as signal modifier $\mu$ for a $3\,\mathrm{ab}^{-1}$ LHC assuming a branching ratio of unity.

| $m_H$ [GeV] | 200 | 300 | 400 | 500 | 600 | 700 | 800 | 900 | 1000 |
|---|---|---|---|---|---|---|---|---|---|
| cut and count | 10 | 6.7 | 4.8 | 3.7 | 2.8 | 2.2 | 1.7 | 1.3 | 1.0 |
| Fisher discriminant | 12 | 8.2 | 5.7 | 4.3 | 3.3 | 2.5 | 1.9 | 1.5 | 1.2 |
| BDT | 13 | 8.8 | 6.4 | 4.8 | 3.6 | 2.8 | 2.2 | 1.7 | 1.3 |

TABLE V: Discovery significance $S/\sqrt{S+B}$ at a $3\,\mathrm{ab}^{-1}$ LHC of our cut and count analysis compared to a Fisher discriminant and a BDT for different Higgs mass parameters $m_{H^{\pm\pm}}$. Both multivariate analyses use the same observables as presented in our cut and count analysis.

### C. Statement of Optimality

When constructing a cut and count analysis it might happen that useful correlations are not considered. To compute the information which is accessible when including correlations, we compute the discovery significance $S/\sqrt{S+B}$ for a $3\,\mathrm{ab}^{-1}$ LHC using the Fisher discriminant as implemented in TMVA [79, 80]. In short, the Fisher discriminant uses the mean value of signal and background as computed on the domain of observables fed in. A hyperplane sliding along the line defined by these two points represents a well defined cut. Therefore, the Fisher discriminant is sensitive to linear correlations. However, if the means coincide it has no sensitivity at all even if the shapes of signal and background differ dramatically. Using a boosted decision tree (BDT), which is also implemented in TMVA, instead helps identifying such cases. In a nutshell, a BDT covers the phase space, as parametrised by the observables we define, with cuboid baskets. These baskets are assigned either to be background or to be signal. This way irregularly shaped backgrounds or signals can be taken into account. Note, that usually one cannot easily train a BDT or Fisher discriminant from MC and use it in an analysis straightforwardly; the propagation of systematic uncertainties must be taken into account. When there is no connection to data, as is the case for this purely MC study, this is hard to do and we stress that we use this tool rather to judge the potential reach of the observables we have chosen to study. In addition, one should add that there might exist observables with better discriminating power than the ones we have chosen so far. The best discriminating power in identifying these is by comparing sensitivity yields to the matrix element method [81, 82], which is by construction the most discriminating observable between two specified signal and background hypotheses. Available tools like MadMax [83], MadWeight [84], shower and event deconstruction [85, 86] have demonstrated their potential in phenomenological analyses [87–92] and extensions to higher-order matrix elements have been proposed [93–95]. The set of observables we use for a proof-of-principle investigation of the sensitivity reach that can be obtained with these methods are the ones defined in the previous section. The event selection is given by Eq. (12). Our results as computed by TMVA are presented in Tab. V. For the Fisher discriminant as well as the BDT we observe a constant enhancement as function of the Higgs mass compared to our cut and count analysis of the previous section. Translated into branching ratios this means that with the help of a BDT, for example, we could reach 10% better upper bounds than stated in Tab. IV. In addition the discovery reach for the LHC cannot be pushed much further than $m_{H^{\pm\pm}} = 800$ GeV, even when accepting the results of a BDT. There is one exception, namely the $300 - 400$ GeV mass region. The numbers quoted in Tab. V indicate 20% better bounds on $\mathrm{BR}(H^{\pm\pm} \to W^{\pm}W^{\pm})$ then Tab. IV.

We stress that the dominating background here is of reducible nature. Indeed, it is dominated by QCD radiation and can therefore be determined relying on data-driven methods. Due to this fact it might be possible to train the Fisher discriminant or a BDT on data [96]. In that case the approach would be robust concerning systematic uncertainties.

### D. Interpretation of results in composite scenarios

Let us finally estimate the impact of the above search on the parameters space of the composite Higgs scenarios as discussed in Sec. II.

Following [17], the couplings of the top partners to the $W$ bosons in the limit of $\chi = v^2/f^2 \ll 1$, with $f$ denoting the analogue of the pion decay constant, carries a factor $\sim e/(2\sqrt{2}\sin\theta_w)$. Small values if $\chi$ are favored by current data [97]. The extension of [17] does not modify the bulk of the 125 GeV Higgs phenomenology and the smallness of this parameter as inferred from, e.g. $H \to ZZ$ observations directly generalises to our case.

The dominant contribution to the loop induced decay is then given by the mass scale set by the top partners as well as the angle that lifts the left-handed bottom mass and "rotates in" the bottom partner to the vertex of Eq. (7). We will denote this angle with $\sin\lambda$ (see again [17] for details). For illustration purposes we identify $M_B = M_{T_1} = M_X$ and focus on the contribution of the lowest lying top partner which will be the numerically least suppressed contribution.

With these assumptions, the effective $H^{\pm\pm} \to W^{\pm}W^{\pm}$ interactions can be parametrised by matching the Lorentz structure to an effective Lagrangian in terms of a power series in a single scale $\sim M_X^{-n}$. Keeping operators up to dimension five, we obtain

$$\mathcal{L}_{\text{eff}} = \frac{\alpha}{128\pi} \frac{\lambda_q \sin\lambda}{\sin^2\theta_w} \frac{H^{--}}{M_x} \big( 2\, W^{+\mu\nu} W^+_{\mu\nu} - 3\, W^{+\mu\nu} \widetilde{W}^+_{\mu\nu} \\ - 4m_W^2 W^{+\mu} W^+_\mu \big) + \text{h.c.} \quad (24)$$

In addition, the potential presence of a Wess-Zumino-Witten term [98, 99] would lead to the presence of the effective interaction [35]

$$\mathcal{L}_{\text{WZW}} = c_{\text{WZW}} \frac{e^2}{16\pi^2 f \sin^2\theta_w} H^{--} W^{+\mu\nu} \widetilde{W}^+_{\mu\nu}, \quad (25)$$

where the coefficient $c_{\text{WZW}}$ relates to combination of invariants of the hyper colour group of Eq. (1) and potential mixing angles as detailed in [35].
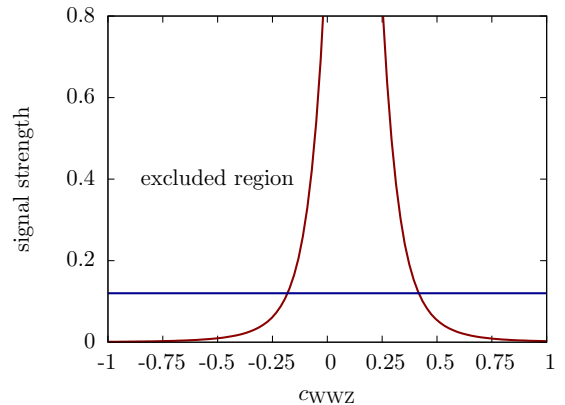


FIG. 7: The signal strength as a function of the Wess-Zumino-Witten interaction of Eq. (25) for representative values $m_{H^{\pm\pm}} = 200$ GeV, $f = M_X = 2$ TeV, $\lambda_q = 2\pi$ and $\sin\lambda = 0.1$.

Assuming a large scale separation $f \sim M$ for illustration, the projections of Tab. IV allow us to set a constraint $-0.18 < c_{\text{WZW}} < 0.42$ as demonstrated in Fig. 7 for the most sensitive case of 200 GeV.** We leave a more dedicated analysis of the impact of this search onto the underlying UV parameters to future work, however, Fig. 7 clearly shows that sensitivity in $l^+ l^+ l^- l^-\,\slashed{E}_T$ provides important information if a composite nature of the TeV scale will be established.

## V. CONCLUSION

In this paper we present a detailed study of doubly charged Higgs production in the limit where the underlying complex triplet has no relation with electroweak symmetry breaking. In particular, observing such a particle in its decay to same sign $W$ bosons will provide important information that might clarify a potential composite nature of the TeV scale.

We have focussed on 13 TeV LHC collisions and extrapolate to high luminosity to gauge the extent to which such states can be observed at the LHC. We have used various analysis strategies to give a more fine-grained picture of the sensitivity that can be reached in the light of a small expected inclusive signal. Assuming $\text{BR}(H^{\pm\pm} \to W^{\pm}W^{\pm}) \equiv 1.0$ we find that the LHC is sensitive to heavy Higgs masses up to about 800 GeV. A high luminosity LHC of $3\,\text{ab}^{-1}$ is able to constrain this decay channel for branching ratios of $\sim 0.44$ for $m_{H^{\pm\pm}} = 200$ GeV growing up to $\sim 0.84$ for $m_{H^{\pm\pm}} = 600$ GeV using a typical cut and count analysis. We have demonstrated that using a BDT much better results might be possible, but only for the mass regime between $300 - 400$ GeV. Considering the reducible nature of the dominating background we encourage experiments to explore this possibility with a data driven strategy.

A limiting factor of this rather clean, yet rare final state is the influence of electron charge flips in the high $p_T$ regime and our scenario provides a motivation to study these effects in same sign, same flavour leptons on the $Z$ mass pole in association with a high $p_T$ jet.

## Acknowledgments

---

** This is only an approximation because it is difficult to phenomenologically disentangle the different Lorentz structures of Eq. (24).

---

[1] J. Gasser and H. Leutwyler, Nucl. Phys. **B250**, 465 (1985).

[2] H. Leutwyler, *Theoretical Advanced Study Institute in Elementary Particle Physics (TASI 91): Perspectives in the Standard Model Boulder, Colorado, June 2-28, 1991*, , 97 (1991), [Lect. Notes Phys.396,1(1991)].

[3] H. Leutwyler, Annals Phys. **235**, 165 (1994), arXiv:hep-ph/9311274 [hep-ph] .

[4] R. Contino, in *Physics of the large and the small, TASI 09, proceedings of the Theoretical Advanced Study Institute in Elementary Particle Physics, Boulder, Colorado, USA, 1-26 June 2009* (2011) pp. 235–306, arXiv:1005.4269 [hep-ph] .

[5] R. Contino, Y. Nomura, and A. Pomarol, Nucl. Phys. **B671**, 148 (2003), arXiv:hep-ph/0306259 [hep-ph] .

[6] R. Contino, T. Kramer, M. Son, and R. Sundrum, JHEP **05**, 074 (2007), arXiv:hep-ph/0612180 [hep-ph] .

[7] K. Agashe, R. Contino, and A. Pomarol, Nucl. Phys. **B719**, 165 (2005), arXiv:hep-ph/0412089 [hep-ph] .

[8] M. Gillioz, R. Grober, C. Grojean, M. Muhlleitner, and E. Salvioni, JHEP **10**, 004 (2012), arXiv:1206.7120 [hep-ph] .

[9] G. F. Giudice, C. Grojean, A. Pomarol, and R. Rattazzi, JHEP **06**, 045 (2007), arXiv:hep-ph/0703164 [hep-ph] .

[10] A. F. Faedo, M. Piai, and D. Schofield, Nucl. Phys. **B880**, 504 (2014), arXiv:1312.2793 [hep-th] .

[11] A. Athenodorou, E. Bennett, G. Bergner, D. Elander, C. J. D. Lin, B. Lucini, and M. Piai, JHEP **06**, 114 (2016), arXiv:1605.04258 [hep-th] .

[12] M. Golterman and Y. Shamir, Phys. Rev. **D91**, 094506 (2015), arXiv:1502.00390 [hep-ph] .

[13] T. DeGrand, Rev. Mod. Phys. **88**, 015001 (2016), arXiv:1510.05018 [hep-ph] .

[14] T. A. DeGrand, M. Golterman, W. I. Jay, E. T. Neil, Y. Shamir, and B. Svetitsky, Phys. Rev. **D94**, 054501 (2016), arXiv:1606.02695 [hep-lat] .

[15] G. Ferretti and D. Karateev, JHEP **03**, 077 (2014), arXiv:1312.5330 [hep-ph] .

[16] J. Barnard, T. Gherghetta, and T. S. Ray, JHEP **02**, 002 (2014), arXiv:1311.6562 [hep-ph] .

[17] G. Ferretti, JHEP **06**, 142 (2014), arXiv:1404.7137 [hep-ph] .

[18] G. von Gersdorff, E. Pontn, and R. Rosenfeld, JHEP **06**, 119 (2015), arXiv:1502.07340 [hep-ph] .

[19] G. Cacciapaglia, H. Cai, A. Deandrea, T. Flacke, S. J. Lee, and A. Parolini, JHEP **11**, 201 (2015), arXiv:1507.02283 [hep-ph] .

[20] A. Belyaev, G. Cacciapaglia, H. Cai, G. Ferretti, T. Flacke, A. Parolini, and H. Serodio, (2016), arXiv:1610.06591 [hep-ph] .

[21] K. Agashe, R. Contino, L. Da Rold, and A. Pomarol, Phys. Lett. **B641**, 62 (2006), arXiv:hep-ph/0605341 [hep-ph] .

[22] J. Mrazek, A. Pomarol, R. Rattazzi, M. Redi, J. Serra, and A. Wulzer, Nucl. Phys. **B853**, 1 (2011), arXiv:1105.5403 [hep-ph] .

[23] A. G. Akeroyd and C.-W. Chiang, Phys. Rev. **D80**, 113010 (2009), arXiv:0909.4419 [hep-ph] .

[24] A. G. Akeroyd, C.-W. Chiang, and N. Gaur, JHEP **11**, 005 (2010), arXiv:1009.2780 [hep-ph] .

[25] H. Georgi and M. Machacek, Nucl. Phys. **B262**, 463 (1985).

[26] M. S. Chanowitz and M. Golden, Phys. Lett. **B165**, 105 (1985).

[27] J. F. Gunion, R. Vega, and J. Wudka, Phys. Rev. **D42**, 1673 (1990).

[28] C. Englert, E. Re, and M. Spannowsky, Phys. Rev. **D88**, 035024 (2013), arXiv:1306.6228 [hep-ph] .

[29] G. Bambhaniya, J. Chakrabortty, J. Gluza, T. Jelinski, and R. Szafron, Phys. Rev. **D92**, 015016 (2015), arXiv:1504.03999 [hep-ph] .

[30] H. E. Logan and V. Rentala, Phys. Rev. **D92**, 075011 (2015), arXiv:1502.01275 [hep-ph] .

[31] Z. Kang, J. Li, T. Li, Y. Liu, and G.-Z. Ning, Eur. Phys. J. **C75**, 574 (2015), arXiv:1404.5207 [hep-ph] .

[32] B. Grinstein, C. W. Murphy, D. Pirtskhalava, and P. Uttayarat, JHEP **05**, 083 (2014), arXiv:1401.0070 [hep-ph] .

[33] S. Fichet, G. von Gersdorff, E. Pontn, and R. Rosenfeld, JHEP **09**, 158 (2016), arXiv:1607.03125 [hep-ph] .

[34] S. Fichet, G. von Gersdorff, E. Pontn, and R. Rosenfeld, JHEP **01**, 012 (2017), arXiv:1608.01995 [hep-ph] .

[35] G. Ferretti, JHEP **06**, 107 (2016), arXiv:1604.06467 [hep-ph] .

[36] C. Kilic, T. Okui, and R. Sundrum, JHEP **02**, 018 (2010), arXiv:0906.0577 [hep-ph] .

[37] C. Kilic and T. Okui, JHEP **04**, 128 (2010), arXiv:1001.4526 [hep-ph] .

[38] S. Schumann, A. Renaud, and D. Zerwas, JHEP **09**, 074 (2011), arXiv:1108.2957 [hep-ph] .

[39] R. Contino, L. Da Rold, and A. Pomarol, Phys. Rev. **D75**, 055014 (2007), arXiv:hep-ph/0612048 [hep-ph] .

[40] S. R. Coleman and E. J. Weinberg, Phys. Rev. **D7**, 1888 (1973).

[41] A. G. Akeroyd and M. Aoki, Phys. Rev. **D72**, 035011 (2005), arXiv:hep-ph/0506176 [hep-ph] .

[42] J. F. Gunion, R. Vega, and J. Wudka, Phys. Rev. **D43**, 2322 (1991).

[43] S. Godfrey and K. Moats, Phys. Rev. **D81**, 075026 (2010), arXiv:1003.3033 [hep-ph] .

[44] K. Cheung and D. K. Ghosh, JHEP **11**, 048 (2002), arXiv:hep-ph/0208254 [hep-ph] .

[45] C. Degrande, K. Hartling, H. E. Logan, A. D. Peterson, and M. Zaro, Phys. Rev. **D93**, 035004 (2016), arXiv:1512.01243 [hep-ph] .

[46] D. B. Kaplan, Nucl. Phys. **B365**, 259 (1991).

[47] A. Azatov, R. Contino, A. Di Iura, and J. Galloway, Phys. Rev. **D88**, 075019 (2013), arXiv:1308.2676 [hep-ph] .

[48] O. Matsedonskyi, G. Panico, and A. Wulzer, JHEP **04**, 003 (2016), arXiv:1512.04356 [hep-ph] .

[49] S. Kanemura, K. Yagyu, and H. Yokoya, Phys. Lett. **B726**, 316 (2013), arXiv:1305.2383 [hep-ph] .

[50] S. Kanemura, M. Kikuchi, K. Yagyu, and H. Yokoya, Phys. Rev. **D90**, 115018 (2014), arXiv:1407.6547 [hep-ph] .

[51] *Performance assumptions for an upgraded ATLAS detector at a High-Luminosity LHC*, Tech. Rep. ATL-PHYS-PUB-2013-004 (CERN, Geneva, 2013).

[52] M. Cacciari, G. P. Salam, and G. Soyez, Eur. Phys. J. **C72**, 1896 (2012), arXiv:1111.6097 [hep-ph] .

[53] *Expected performance of the ATLAS b-tagging algorithms in Run-2*, Tech. Rep. ATL-PHYS-PUB-2015-022 (CERN, Geneva, 2015).

[54] G. Piacquadio and C. Weiser, *Proceedings, 16th International Conference on Computing in High Energy and Nuclear Physics (CHEP 2007): Victoria, Canada, September 2-7, 2007*, J. Phys. Conf. Ser. **119**, 032032 (2008).

[55] C. Englert, M. Spannowsky, and C. Wymant, Phys. Lett. **B718**, 538 (2012), arXiv:1209.0494 [hep-ph] .

[56] G. Aad *et al.* (ATLAS), JINST **3**, S08003 (2008).

[57] J. Alwall, M. Herquet, F. Maltoni, O. Mattelaer, and T. Stelzer, JHEP **06**, 128 (2011), arXiv:1106.0522 [hep-ph] .

[58] J. Alwall, R. Frederix, S. Frixione, V. Hirschi, F. Maltoni, O. Mattelaer, H. S. Shao, T. Stelzer, P. Torrielli, and M. Zaro, JHEP **07**, 079 (2014), arXiv:1405.0301 [hep-ph] .

[59] J. Bellm *et al.*, Eur. Phys. J. **C76**, 196 (2016), arXiv:1512.01178 [hep-ph] .

[60] S. Gieseke, P. Stephens, and B. Webber, JHEP **12**, 045 (2003), arXiv:hep-ph/0310083 [hep-ph] .

[61] K. Hamilton and P. Richardson, JHEP **02**, 069 (2007), arXiv:hep-ph/0612236 [hep-ph] .

[62] M. Bahr *et al.*, Eur. Phys. J. **C58**, 639 (2008), arXiv:0803.0883 [hep-ph] .

[63] M. A. Gigg and P. Richardson, (2008), arXiv:0805.3037 [hep-ph] .

[64] G. Altarelli, R. K. Ellis, and G. Martinelli, Nucl. Phys. **B143**, 521 (1978), [Erratum: Nucl. Phys.B146,544(1978)].

[65] M. Muhlleitner and M. Spira, Phys. Rev. **D68**, 117701 (2003), arXiv:hep-ph/0305288 [hep-ph] .

[66] V. Hankele and D. Zeppenfeld, Phys. Lett. **B661**, 103 (2008), arXiv:0712.3544 [hep-ph] .

[67] G. Bozzi, F. Campanario, V. Hankele, and D. Zeppenfeld, Phys. Rev. **D81**, 094030 (2010), arXiv:0911.0438 [hep-ph] .

[68] F. Campanario, V. Hankele, C. Oleari, S. Prestel, and D. Zeppenfeld, Phys. Rev. **D78**, 094012 (2008), arXiv:0809.0790 [hep-ph] .

[69] J. M. Campbell, R. K. Ellis, and C. Williams, JHEP **07**, 018 (2011), arXiv:1105.0020 [hep-ph] .

[70] M. Grazzini, S. Kallweit, and D. Rathlev, Phys. Lett. **B750**, 407 (2015), arXiv:1507.06257 [hep-ph] .

[71] F. Campanario, C. Englert, S. Kallweit, M. Spannowsky, and D. Zeppenfeld, JHEP **07**, 076 (2010), arXiv:1006.0390 [hep-ph] .

[72] F. Campanario, C. Englert, M. Spannowsky, and D. Zeppenfeld, Europhys. Lett. **88**, 11001 (2009), arXiv:0908.1638 [hep-ph] .

[73] C. Englert, T. Plehn, P. Schichtel, and S. Schumann, Phys. Rev. **D83**, 095009 (2011), arXiv:1102.4615 [hep-ph] .

[74] E. Gerwick, T. Plehn, and S. Schumann, Phys. Rev. Lett. **108**, 032003 (2012), arXiv:1108.3335 [hep-ph] .

[75] E. Gerwick, T. Plehn, S. Schumann, and P. Schichtel, JHEP **10**, 162 (2012), arXiv:1208.3676 [hep-ph] .

[76] C. Englert, T. Plehn, P. Schichtel, and S. Schumann, JHEP **02**, 030 (2012), arXiv:1108.5473 [hep-ph] .

[77] T. Plehn, D. L. Rainwater, and D. Zeppenfeld, Phys. Rev. **D61**, 093005 (2000), arXiv:hep-ph/9911385 [hep-ph] .

[78] N. Kauer, T. Plehn, D. L. Rainwater, and D. Zeppenfeld, Phys. Lett. **B503**, 113 (2001), arXiv:hep-ph/0012351 [hep-ph] .

[79] A. Hocker *et al.*, *Proceedings, 11th International Workshop on Advanced computing and analysis techniques in physics research (ACAT 2007): Amsterdam, Netherlands, April 23-27, 2007*, PoS **ACAT**, 040 (2007), arXiv:physics/0703039 [PHYSICS] .

[80] P. Speckmayer, A. Hocker, J. Stelzer, and H. Voss, *Proceedings, 17th International Conference on Computing in High Energy and Nuclear Physics (CHEP 2009): Prague, Czech Republic, March 21-27, 2009*, J. Phys. Conf. Ser. **219**, 032057 (2010).

[81] K. Kondo, J. Phys. Soc. Jap. **57**, 4126 (1988).

[82] V. M. Abazov *et al.* (D0), Nature **429**, 638 (2004), arXiv:hep-ex/0406031 [hep-ex] .

[83] T. Plehn, P. Schichtel, and D. Wiegand, Phys. Rev. **D89**, 054002 (2014), arXiv:1311.2591 [hep-ph] .

[84] P. Artoisenet, V. Lemaitre, F. Maltoni, and O. Mattelaer, JHEP **12**, 068 (2010), arXiv:1007.3300 [hep-ph] .

[85] D. E. Soper and M. Spannowsky, Phys. Rev. **D84**, 074002 (2011), arXiv:1102.3480 [hep-ph] .

[86] D. E. Soper and M. Spannowsky, Phys. Rev. **D89**, 094005 (2014), arXiv:1402.1189 [hep-ph] .

[87] D. E. Soper and M. Spannowsky, Phys. Rev. **D87**, 054012 (2013), arXiv:1211.3140 [hep-ph] .

[88] G. Aad *et al.* (ATLAS), JHEP **06**, 093 (2016), arXiv:1603.03127 [hep-ex] .

[89] C. Englert, O. Mattelaer, and M. Spannowsky, Phys. Lett. **B756**, 103 (2016), arXiv:1512.03429 [hep-ph] .

[90] V. Khachatryan *et al.* (CMS), Phys. Lett. **B758**, 321 (2016), arXiv:1511.06170 [hep-ex] .

[91] F. Kling, T. Plehn, and P. Schichtel, Submitted to: Phys. Rev. D (2016), arXiv:1607.07441 [hep-ph] .

[92] D. Ferreira de Lima, P. Petrov, D. Soper, and M. Spannowsky, (2016), arXiv:1607.06031 [hep-ph] .

[93] J. M. Campbell, W. T. Giele, and C. Williams, JHEP **11**, 043 (2012), arXiv:1204.4424 [hep-ph] .

[94] T. Martini and P. Uwer, JHEP **09**, 083 (2015), arXiv:1506.08798 [hep-ph] .

[95] A. V. Gritsan, R. Rntsch, M. Schulze, and M. Xiao, Phys. Rev. **D94**, 055023 (2016), arXiv:1606.03107 [hep-ph] .

[96] C. Bernaciak, T. Plehn, P. Schichtel, and J. Tattersall, Phys. Rev. **D91**, 035024 (2015), arXiv:1411.7699 [hep-ph] .

[97] G. Aad *et al.* (ATLAS), JHEP **11**, 206 (2015), arXiv:1509.00672 [hep-ex] .

[98] J. Wess and B. Zumino, Phys. Lett. **B37**, 95 (1971).

[99] E. Witten, Nucl. Phys. **B223**, 422 (1983).